

5/3-34
27-17

Turbulence modeling for non-equilibrium flow

By P. A. Durbin

1. Motivation and objectives

The work performed during this year has involved further assessment and extension of the $k - \varepsilon - v^2$ model, and initiation of work on scalar transport. The latter is introduced by the contribution of Y. Shabany to this volume.

Flexible, computationally tractable models are needed for engineering CFD. As computational technology has progressed, the ability and need to use elaborate turbulence closure models has increased. The objective of our work is to explore and develop new analytical frameworks that might extend the applicability of the modeling techniques. In past years the development of a method for near-wall modeling was described. The method has been implemented into a CFD code and its viability has been demonstrated by various test cases. Further tests are reported herein.

Non-equilibrium near-wall models are needed for some heat transfer applications. Scalar transport seems generally to be more sensitive to non-equilibrium effects than is momentum transport. For some applications turbulence anisotropy plays a role and an estimate of the full Reynolds stress tensor is needed. We have begun work on scalar transport *per se*, but in this brief I will only report on an extension of the $k - \varepsilon - v^2$ model to predict the Reynolds stress tensor. The $k - \varepsilon - v^2$ model contains a representation of anisotropy via the k and $\overline{v^2}$ velocity scales. By invoking an algebraic stress approximation a formula can be derived to relate the stress tensor $\overline{u_i u_j}$ to k , $\overline{v^2}$ and $\partial_j U_i$.

2. Accomplishments

The governing equations of the $k - \varepsilon - v^2$ model will not be presented here. They can be found in Durbin (1995a). The mean flow satisfies the incompressible Navier-Stokes equations with an eddy viscosity. The turbulence model uses the standard $k - \varepsilon$ equations, a $\overline{v^2}$ transport equation, and an elliptic relaxation equation for the source term (f_{22}) in the $\overline{v^2}$ -equation.

Subroutines were written to extend the INS-2D code of Rogers and Kwak (1990) to axisymmetric flow, including swirl. The flows computed with this extended code are a confined coaxial jet, with and without swirl, and an impinging circular jet. The former is a test case for certain combustor flows; the latter is relevant to impingement cooling.

2.1 Confined coaxial jets

The geometry is illustrated by Fig. 1. The upstream section is a coaxial pipe that dumps into a larger cylinder. Inlet profiles were created by computing fully developed pipe flow. This is the correct condition for the non-swirling experiment of

Habib and Whitelaw (1979). The swirling flow experiment of Roback and Johnson (1983) was not fully developed at the inlet. Indeed, it was necessary to contrive a swirl distribution within the pipe that would reproduce the swirl measured at the first measurement station in the experiment.

Figure 2 shows the computational and experimental results for the centerline velocity for 1:1 and 3:1 peak velocity ratios of the coaxial jets. This illustrates that the model predicts reasonable entrainment rates for the axisymmetric jet.

Swirling flow computations are contained in Fig. 3. It is possible to derive a swirl contribution to the turbulence model by regarding $\overline{v^2}$ as the radial component of the Reynolds normal stress. The solid line has this correction, the dashed line does not. It can be seen that the swirl effect on the turbulence is not important. As plotted, the experimental data do not conserve mass flux—they probably should be rescaled. However, the second profile shows that there is considerable scatter in the measurements.

The streamwise extent and radial height of the backflow region is well predicted by the model. Of course, the existence of the backflow bubble is a product of the Navier-Stokes equations; but the size of the bubble is controlled by how the turbulent entrainment is modeled. Also the model is responsible for the existence of a (statistically) steady, stable solution to the equations.

2.2 Impinging jet

The stagnation point jet is a flow in which some standard turbulence models have failed dramatically. The key features of this flow are both the large total strain along the stagnation streamline and the mean flow being perpendicular to the surface. A virtue of the elliptic relaxation method is that the governing equations and boundary conditions automatically distinguish the normal component of turbulent intensity. Damping functions for Reynolds stress models have failed in this flow because they assumed the mean flow to be tangent to the surface.

The large strain produces a ‘stagnation point anomaly’ (Durbin 1996) in the $k - \varepsilon$ and $k - \omega$ types of model. We did not experience that difficulty with the $k - \varepsilon - v^2$ model, but the underlying use of the standard $k - \varepsilon$ system will produce anomalous behavior in more strongly strained flows. Figure 5 shows the anomalously high heat transfer coefficient obtained with the $k - \varepsilon$ model and the more reasonable results with $k - \varepsilon - v^2$. The data are from Cooper *et al.* (1993).

The origin of the different behaviors of these models is explained by Fig. 6. This shows hot wire data for the streamwise intensity along the stagnation point streamline along with predictions of k and v^2 . The overprediction of St by $k - \varepsilon$ is due to using k , instead of the normal component, for the transport velocity scale, coupled to an overprediction of k .

2.4 Algebraic stress model

In applications of eddy diffusion to passive scalar transport, it is sometimes necessary to represent the anisotropy of the turbulence. For instance, near a wall, the turbulent diffusivity tangential to the surface can be an order of magnitude larger than that in the normal direction. The $k - \varepsilon - v^2$ eddy viscosity, $C_\mu \overline{v^2} T$

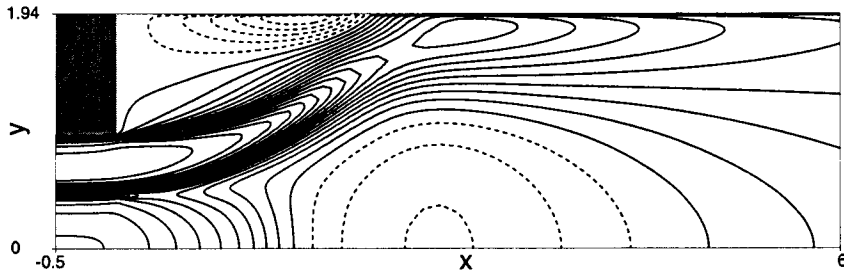


FIGURE 1. Contours of constant u -velocity for swirling, confined coaxial jet, showing a backflow bubble on the axis: $S=0.47$ corresponding to the Johnson and Roback experiment.

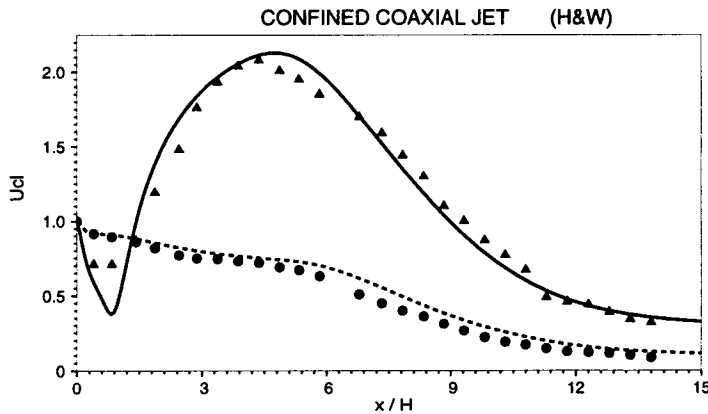


FIGURE 2. Centerline velocities for non-swirling coaxial jets. Data from Habib and Whitelaw. \bullet , jet velocity ratio=1; \blacktriangle , jet velocity ratio=3; curves=model.

(T is the turbulence time-scale, k/ϵ at high Reynolds number), describes transport in the normal direction, which is usually suitable for solving the mean momentum equation. However, if there is a concentrated heat source on the surface, then heat transport in the streamwise direction can be important. This type of application requires that the full Reynolds stress tensor be estimated, using the more limited information predicted by the model.

A potential advantage of the $k - \epsilon - \overline{v^2}$ over the $k - \epsilon$ model is that $\overline{v^2}/k$ provides a measure of anisotropy. Of course, the crucial role of anisotropy near walls was the original motivation for $k - \epsilon - \overline{v^2}$: the $\overline{v^2}$ -equation enables the model to be integrated to the wall without damping functions because it acknowledges this important property of the turbulence. Here the anisotropic nature of this model will be exploited further: an algebraic formula to predict the other components of the Reynolds stress tensor from knowledge of k , ϵ , and $\overline{v^2}$ will be proposed.

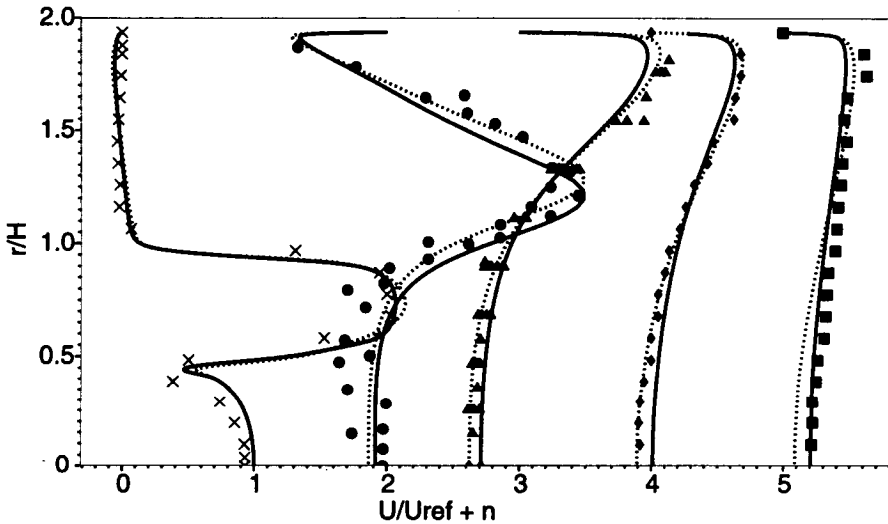


FIGURE 3. Mean velocity profiles for the swirling jet with experimental data. The origin of the first velocity profile is at 0, the others are displaced to 2,3,4,5. Hence the second, third and fourth profiles show backflow on the axis, in agreement with the experiment. Data from Johnson and Roback. The dashed lines were computed with the basic model, the solid lines have a swirl term added to the v^2 -equation.

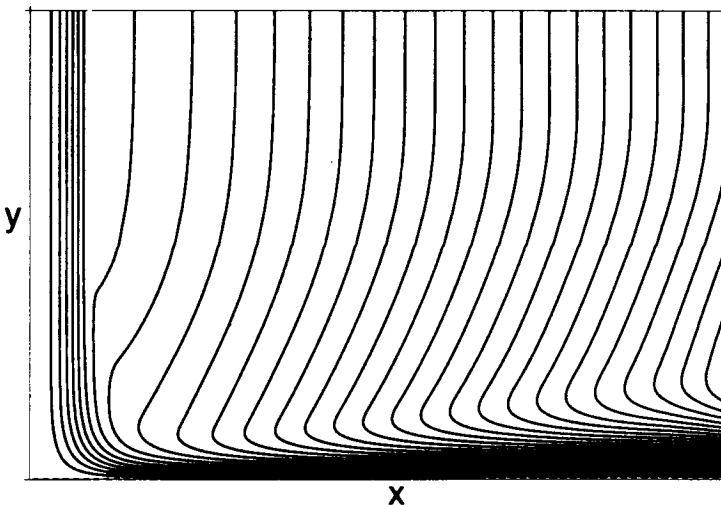


FIGURE 4. Streamlines for an axisymmetric jet impinging on a plane wall.

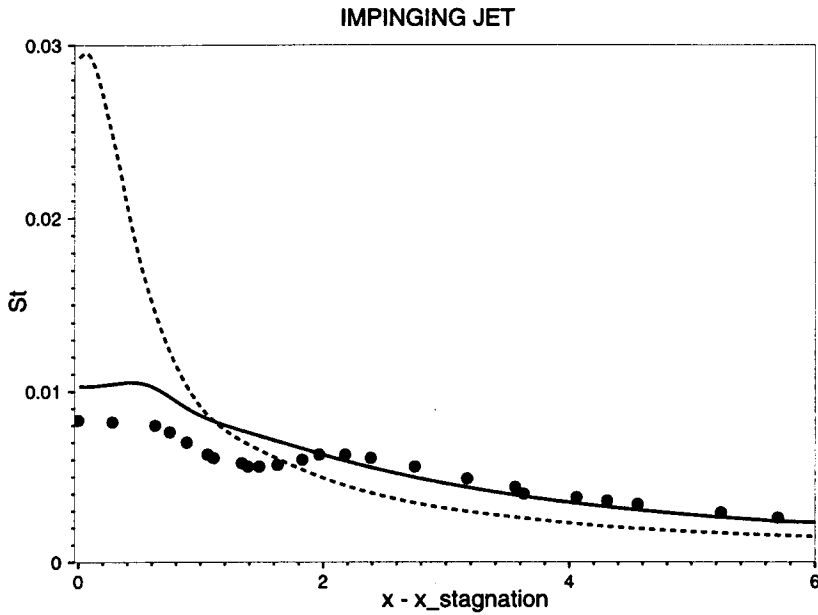


FIGURE 5. Stanton number versus radial distance along the impingement wall. The dashed line illustrates the stagnation point anomaly observed with the standard $k - \epsilon$ model + wall damping function. The $k - \epsilon - v^2$ model does not show that anomaly in this flow.

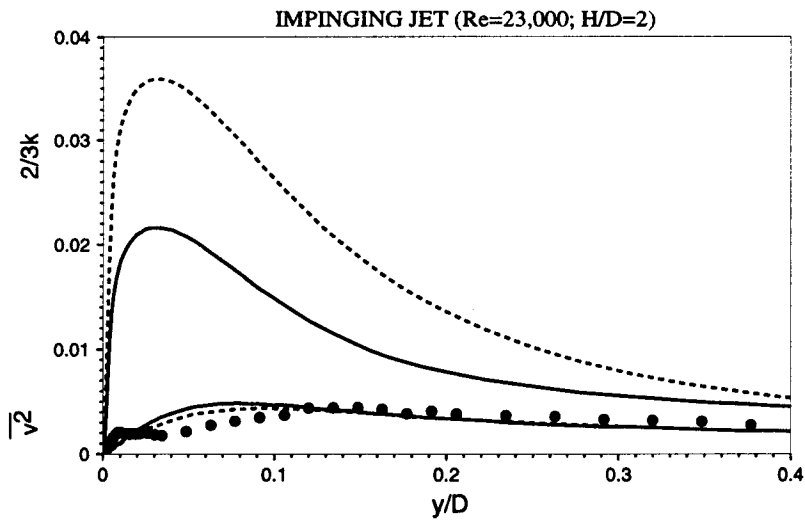


FIGURE 6. Single wire measurements of streamwise velocity fluctuations on the stagnation streamline with model prediction of $\overline{v^2}$ shown by the lower curves. The upper curves show k . The solid curves impose the bound discussed in Durbin (1996).

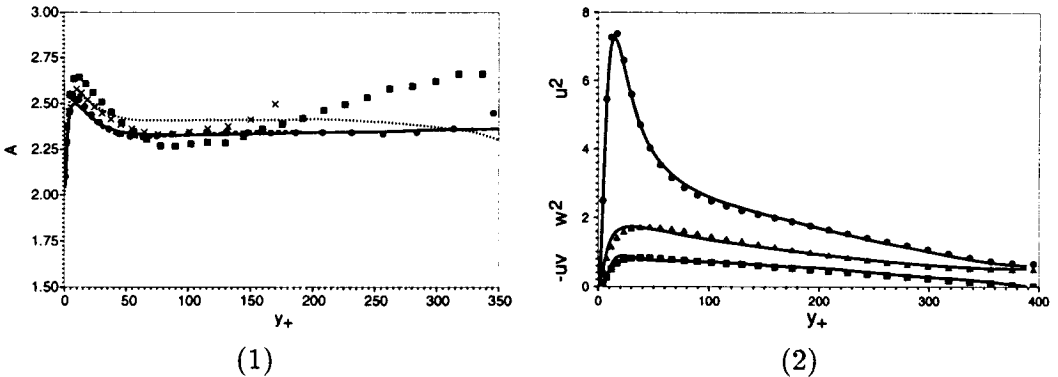


FIGURE 7. (1) Symbols: $A = (\overline{u_1^2} - \overline{u_2^2}) / (2/3 k - \overline{u_2^2})$ from DNS data; Curves: $A = 2 + 6S^* / (15 + 10S^*)$. (2) Reynolds stresses in channel flow, $R_\tau = 395$.

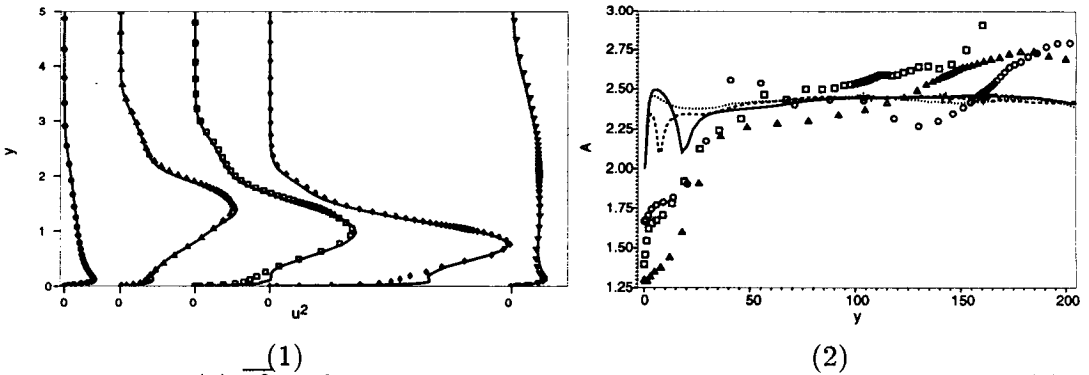


FIGURE 8. (1) $\overline{u^2}$ in flow over a backstep at various downstream positions. (2) Backstep: Symbols: $A = (\overline{u_1^2} - \overline{u_2^2}) / (2/3 k - \overline{u_2^2})$; Curves: $A = 2 + 6S^* / (15 + 10S^*)$

A general constitutive relation that depends additionally on the mean flow gradients is of the form

$$\overline{u_i u_j} = k F_{ij}(\mathbf{I}, \mathbf{S}, \mathbf{\Omega}, \overline{v^2}, k, T) \tag{1}$$

where $S_{ij} = 1/2 (\partial_j U_i + \partial_i U_j)$; $\Omega_{ij} = 1/2 (\partial_j U_i - \partial_i U_j)$ and \mathbf{I} is the identity tensor. For two-dimensional incompressible flow, the most general tensor function of $\mathbf{\Omega}$ and \mathbf{S} can be tailored to present purposes. This leads to the form

$$\begin{aligned} \overline{u_i u_j} = & -2\nu_T S_{ij} + 2/3 k \delta_{ij} \\ & + \left(2/3 k - \overline{v^2} \right) \left[A \left(\frac{\Omega_{ik} S_{kj} - S_{ik} \Omega_{kj}}{|S^2| + |\Omega^2|} \right) + (A - 2) \left(\frac{3S_{ik} S_{kj}}{|S^2|} - \delta_{ij} \right) \right] \end{aligned} \tag{2}$$

where A is a coefficient that can be a function of the invariants $|S^2| = S_{ij} S_{ji}$ and $|\Omega^2| = -\Omega_{ij} \Omega_{ji}$. This is a type of quasi-equilibrium assumption; Durbin (1995b) describes a method to derive this constitutive relation by an equilibrium approximation.

In two-dimensional incompressible, parallel shear flow, $\overline{u_2^2} = \overline{v^2}$ and (2) becomes

$$\overline{u_1^2} = \overline{v^2} + \left(2/3 k - \overline{v^2} \right) A. \tag{3}$$

An assumption commonly made to infer k from cross-wire measurements of $\overline{u_1^2}$ and $\overline{u_2^2}$ is $k = 3/4 (\overline{u_1^2} + \overline{u_2^2})$: this gives $A = 2$. Equation (3) permits A to be evaluated from DNS data as $A = (\overline{u_1^2} - \overline{u_2^2}) / (2/3 k - \overline{u_2^2})$. Figure 7(1) evaluates A from boundary-layer and channel-flow DNS data. A is greater than 2 over the entire flow: a rather better approximation is $A = 2.4$. Correspondingly, a more accurate estimate of k from cross-wire data would be $k \approx (\overline{u_1^2} + 1.4\overline{u_2^2})/1.6$. The function

$$A = 2 + \frac{6S^*}{15 + 10S^*} \quad (4)$$

where $S^* = Sk/\epsilon$, gives a slightly better approximation to the data. In Fig. 7(2) the algebraic model (2) is evaluated for channel flow; DNS data for $\overline{u_1^2}$ in flow over a backward facing step (provided by H. Le) is shown in Fig. 8(1), along with curves obtained from the algebraic model; x -derivatives have been ignored and (4) used. The step is located at $x = 0$ and the reattachment point is at $x = 6$. In the separated shear layer, the algebraic relation between k , $\overline{v^2}$, and $\overline{u_1^2}$ is quite accurate. Near the wall, in the neighborhood of reattachment, the model (4) produces a spurious maximum: this is due to a peak in the anisotropy measure $2/3 k - \overline{v^2}$; neither k or $\overline{v^2}$ themselves show this peak. This illustrates a limitation to the present method of representing anisotropy. Figure 8(2) shows evaluations of A using backstep data. Comparison of the curves and symbols shows how the anisotropic contribution to $\overline{u_1^2}$ is overpredicted near the wall by (4).

REFERENCES

- COOPER, D., JACKSON, D. C., LAUNDER, B. E. & LIAO, G. X. 1993 Impinging jet studies for turbulence model assessment. *Int. J. Heat Mass Transfer.* **36**, 2675–2684
- DURBIN, P. A. 1995a Separated flow computations with the $k - \epsilon - v^2$ model. *AIAA Journal.* **44**, 659–664
- DURBIN, P. A. 1995b Constitutive equation for the $k - \epsilon - v^2$ model. *6th Int. Symp. on CFD*, 258–262
- DURBIN, P. A. 1996 On the $k - \epsilon$ stagnation point anomaly. *Int. J. Heat and Mass Transf.* to appear
- ROGERS, S. E. & KWAK, D. 1990 Upwind differencing scheme for the time-accurate incompressible Navier-Stokes equations. *AIAA Journal.* **28**, 253–262
- HABIB, M. A. & WHITELAW, J. H. 1979 Velocity characteristics of a confined coaxial jet. *ASME J. Fluids Eng.* **101**, 521–529
- ROBACK, R. & JOHNSON, B. V. 1983 Mass and momentum turbulent transport experiments with confined swirling coaxial jets. *NASA CR-168252*